ADVANCED FUNCTIONAL MATERIALS
www.afm-journal.de

Protein/Polymer-Based Dual-Responsive Gold Nanoparticles with pH-Dependent Thermal Sensitivity

Malte S. Strozyk, Munish Chanana, Isabel Pastoriza-Santos, Jorge Pérez-Juste, and Luis M. Liz-Marzán**

This article presents the synthesis and physicochemical behavior of dual-responsive plasmonic nanoparticles with reversible optical properties based on protein-coated gold nanoparticles grafted with thermosensitive polymer brushes by means of surface-initiated atom transfer radical polymerization (SI-ATRP) that exhibit pH-dependent thermo-responsive behavior. Spherical gold NPs of two different sizes (15 nm and 60 nm) and with different stabilizing agents (citrate and cetyltrimethylammonium bromide (CTAB), respectively) were first capped with bovine serum albumin (BSA). The resulting BSA-capped NPs (Au@BSA NPs) exhibited not only extremely high colloidal stability under physiological conditions, but also a reversible U-shaped pH-responsive behavior, similar to pure BSA. The ε-amine of the L-lysine in the protein coating was then used to covalently bind an ATRP-initiator, allowing for the SI-ATRP of thermosensitive polymer brushes of oligo(ethylene glycol) methacrylates with an LCST of 42 °C in pure water and around 37 °C under physiological conditions. Such protein coated nanoparticles grafted with thermosensitive polymers exhibit a smart pH-dependent thermosensitive behavior.

1. Introduction

Stimuli-responsive nanoparticles (NPs) have gained a great deal of attention in the past decade because of their emerging applications,[1] as (bio-)sensors,[2–4] drug delivery systems,[5] and "smart" coatings,[6] due to their sensitivity towards environmental changes[1] that results in a pronounced response, often through volume, porosity or wettability changes.[6–8] Various types of stimuli-responsive nanosystems[8] have been developed, which are highly sensitive towards environmental temperature,[9] pH,[10] heavy metals[11,12] or light.[13] However, the current trends are moving towards stimuli-responsive systems, which are sensitive towards more than one stimulus, resulting in a multiresponsive system.[1,3,8] The responsive behavior of such systems strongly depends on the chemical composition of the organic material. For example, molecules bearing weak acidic or basic functionalities, such as carboxylic or amino groups, impart pH-sensitivity to the particles, due to the changes in ionization degree (protonation/deprotonation) induced by pH changes. Thermo-responsive molecules, such as non-ionic hydrophilic polymers, on the other hand, confer temperature-sensitivity to the particles, due to the hydrophilic/hydrophobic transition induced by temperature changes.

The majority of the multiresponsive nanomaterials that have been developed so far are based on crosslinked hydrogels,[14] self-assembled block-copolymers[15] and inorganic/organic core-shell systems, mostly with an inorganic (metal/metal oxide) core grafted with a multiresponsive organic coating.[16–21] In the latter case, the organic coating usually consists of multiresponsive polymers with various designs, such as block copolymers,[22] random copolymers,[19,20] mixed polymer brushes,[16] crosslinked hydrogels[21] or branched[17,18] and hyper-branched[2] polymers. Especially, in the case of branched polymer systems, semi-synthetic biopolymer/polymer conjugates, where the biopolymer backbone and the synthetic polymer branches are sensitive to different stimuli, are of particular interest.[17] Recently, Zhang et al.[17] and Yuan et al.[18] reported on such semi-synthetic core–shell systems based on gold NPs coated with pH and temperature responsive shells, consisting of dextran/PNIPAAm conjugates or chitosan-g-PDMAEMA copolymers, respectively. However, these biopolymers are not stimuli-responsive *per se* and need to be chemically modified in order to become multiresponsive. Proteins, however, constitute a class of biopolymers that are multiresponsive by nature. Proteins are natural copolymers of polar, nonpolar, and ionic (anionic and cationic) monomers, i.e. aminoacids (in total 21 aminoacids).[23] Depending on both their molecular composition (primary structure) and their conformational structure (secondary and tertiary structures), proteins exhibit not only different biological activities,[23] but also different physical and chemical properties, such as different solubility profiles in various solvents, different isoelectric points (pI) and different denaturation and gelation temperatures.[23–27] Therefore, proteins are highly sensitive to pH,[11,25] temperature,[25] ionic strength,[26] solvent[24] and heavy metals.[11,28]

Malte S. Strozyk, Dr. M. Chanana, Dr. I. Pastoriza-Santos, Dr. J. Pérez-Juste, Prof. L. M. Liz-Marzán
Departamento de Química Física
Universidade de Vigo
Campus Universitario
36310, Vigo, Spain
Tel: +34 9868 18617, Fax: +34 986812556
E-mail: chanana@uvigo.es; lmarzan@uvigo.es

DOI: 10.1002/adfm.201102471

Besides being multiresponsive, proteins are also multifunctional and provide a broad range of molecular and conformational structures as well as a huge variety of chemical functionalities on the same molecule, offering a vast library of functional polymers, which can be grafted on the NPs, imparting them with unique chemical, physical and eventually biological properties. In the literature, several reports can be found dealing with gold NPs directly coated with aminoacids[29] or their oligomers/polymers, i.e. peptides[30] and proteins,[31–33] bovine serum albumin (BSA)[32–34] being the most widely used protein. We recently reported on the properties of colloidal gold NPs coated with insulin (Au@insulin NPs),[11] which is a small hormonal protein (5808 g/mol). Such Au@insulin NPs exhibit not only extremely high colloidal stability in aqueous electrolyte solutions (up to 1 M NaCl), but also a high sensitivity toward environmental pH and the presence of various heavy metal ions. Au@insulin NPs were shown to display pH- and metal-sensitive aggregation behavior, which could be monitored through reversible changes in their optical properties.[11] In general, by changing the environmental pH or temperature, especially at pH = pI or at high temperature, proteins undergo conformational changes resulting in their precipitation and/or denaturation. Whereas the pH-induced conformational changes are mostly reversible,[11] the temperature-induced changes, i.e., denaturation, are mostly irreversible and the proteins usually phase separate from solution.[27,35] Therefore, proteins perfectly qualify as stimuli-responsive coatings, in terms of reversible pH and heavy metal ion sensitivity, but they fail to provide reversible thermal sensitivity.

In the present work, we describe the synthesis of fully reversible pH- and temperature-responsive metal NPs based on a protein/polymer conjugate system. Several reports on protein/polymer conjugates can be found in the literature,[36] but multiresponsive inorganic nanoparticles coated with protein/polymer conjugates have not been reported so far. Hence, we selected proteins as the coating material of NPs because of their unique pH-responsive properties, but also because they present many other advantages, such as robust capping abilities, high colloidal stability and, in particular, the ease of performing further functionalization on the remaining functional groups. In this context, the amine groups of the protein allow for fast and simple reactions based on amide-reaction for introducing desired functionalities in high yield. Using amine chemistry, we coupled an atom transfer radical polymerization (ATRP)-initiator via an amide bond to the protein coated NPs, in order to graft polymer brushes from the particle surface by means of surface-initiated ATRP (SI-ATRP). ATRP is a living radical polymerization method, particularly attractive because of its versatility in the types of monomers and functional groups, solvents (aqueous and non-aqueous), tolerance to impurities and mild reaction conditions.[37] SI-ATRP in particular is a very attractive method, since it allows for controlled polymer grafting exclusively from the particle surface, without creating free polymers in the reaction mixture.[38] There are only few reports in literature on SI-ATRP conducted on particles,[39] such as silica,[40] magnetite[41] and gold NPs.[42] However, most of them comprise complicated and multistep reactions in different types of solvents, which could lead to particle aggregation and thus, poor product quality and quantity. In order to circumvent such problems, we present a facile and green method for the synthesis of multiresponsive NPs in (semi-) aqueous (H_2O/DMF (1:1 v/v)) media, with a minimum number of reaction steps, ensuring high yield and excellent quality of the end product. Therefore, we coated gold NPs with BSA, which conferred not only a U-shaped pH-responsive behavior to the NPs, but also provided high colloidal stability for further reaction steps and ease of creating an ATRP-initiation moiety on the NPs. Subsequently, non-ionic polymer brushes, made of random co-polymers of 2-(2-methoxyethoxy) ethyl methacrylate (MEO_2MA) and oligo (ethylene glycol) methacrylate (OEGMA), with fully reversible thermal response were grafted on the protein-capped NPs via SI-ATRP performed in (semi-)aqueous media. The resulting protein/polymer-coated NPs (Au@protein-*g*-polymer NPs) could be reversibly aggregated and disaggregated with temperature, but interestingly, only at low pH. This feature of the protein/polymer-coated NPs could lead to the development of smart oral drug delivery and diagnostic systems, especially in the field of gastrointestinal diseases. For example, an orally administered drug delivery or diagnostic system based on such a dual-responsive NPs would allow for temperature-controlled drug release or diagnostic response, while passing through different (pH-) regions of the human gastrointestinal tract. Therefore, a pH-dependent thermosensitive drug delivery system that could release the drug exclusively in stomach (low pH) or in the intestines (high pH) triggered by temperature, would find wide applications in biomedicine and oral drug delivery formulations. Hence, protein (BSA) coated nanoparticles grafted with thermosensitive polymers represent a novel multi-functional nanoscale material, which could provide access to stimuli-responsive drug delivery systems and multi-functional diagnostic systems.

2. Results and Discussion

The dual-responsive protein/polymer-coated gold NPs, Au@BSA-*g*-Poly(MEO_2MA-co-OEGMA) NPs, were synthesized according to the synthesis scheme illustrated in **Scheme 1**. Gold NPs were selected in this study, not only because they display optical properties that allow us to monitor aggregation processes, but also because they can be easily synthesized with a tight control on NP size and shape, via different techniques such as the seeded-growth method.[43] Whereas gold NPs stabilized by a weak stabilizer such as citrate provide a simple surface chemistry for their functionalization, such as ligand exchange reactions using e.g., thiols or disulfides, the functionalization of gold NPs stabilized with surfactants such as CTAB (cetyltrimethylammonium bromide) is very delicate and often results into irreversible NP aggregation. Therefore, we used gold NPs made by means of the two most commonly applied synthesis methods, namely the Turkevich method (~15 nm)[44] and the seeded-growth method (~60 nm),[45] using citrate and CTAB as stabilizers, respectively. Thus, a special emphasis was made on showing the flexibility of the method for NPs with different size and surface chemistry.

In the first synthesis step (see Scheme 1), both types of gold NPs were coated with BSA, which is a globular protein with relatively high molecular weight (66776 g/mol). Moreover, BSA has a relatively high content of the thiol-containing aminoacid

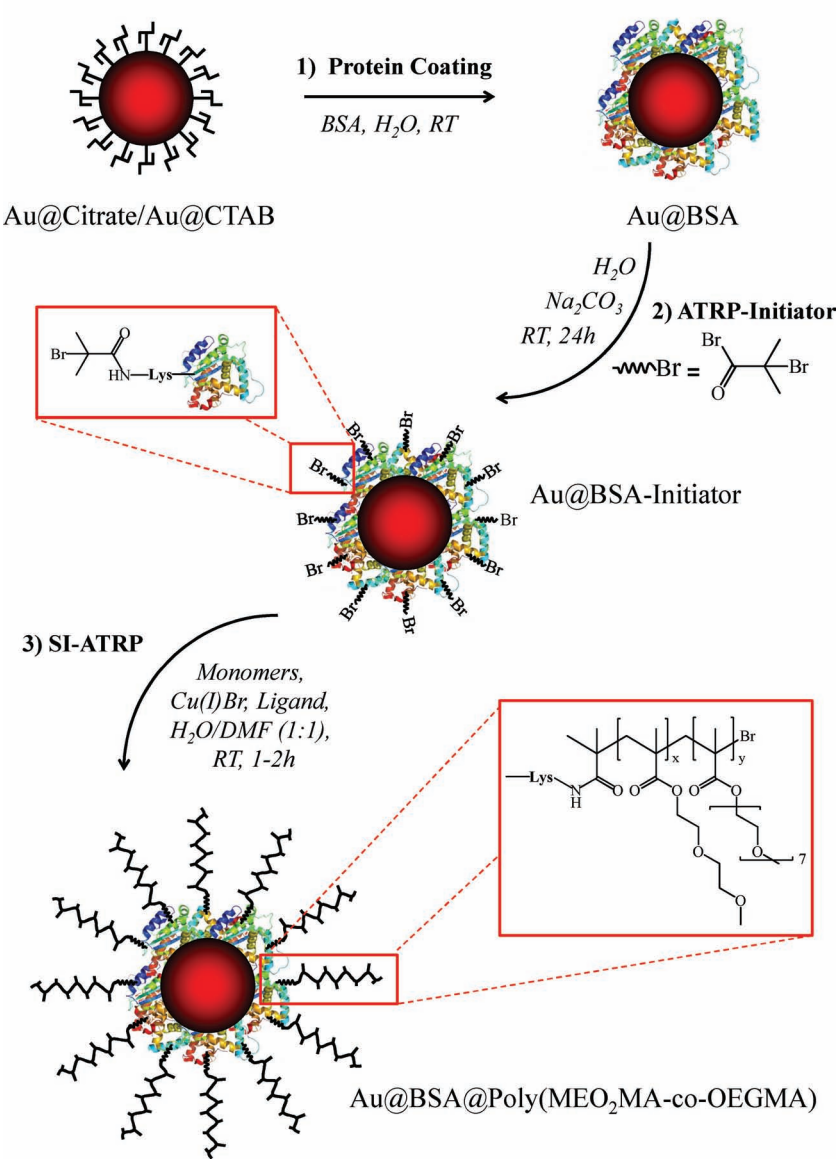

Scheme 1. Complete synthesis route of Au@BSA@Poly(MEO_2MA-co-OEGMA) NPs: 1) Coating Au@citrate or Au@CTAB with BSA (Au@BSA). 2) Coupling ATRP-Initiator to the amine groups (Lysin) of BSA coating (Au@BSA-Ini). 3) Surface-Initiated ATRP on Au@BSA-Ini NPs (Au@BSA@Polymer).

cystein (35xCys), negatively charged aminoacids with carboxylic groups (41xAsp and 48xGlu) and positively charged amino acids with amine (60xLys) and guanidinium (26xArg) groups.[46] These functional groups, especially the thiol/disulfide and the amine groups, can strongly bind to gold NP surfaces, resulting in a very robust capping.[47]

The 15 nm citrate-coated gold NPs[44] (Au15@citrate) were coated with BSA via ligand exchange by simply adding BSA/citrate solution (0.1wt% citrate, $c(BSA)_{final}$ = 0.1 mg/mL) to the as-prepared Au15@citrate NP dispersion at room temperature. The resulting Au15@BSA NPs exhibited a localized surface plasmon resonance (LSPR) band centered around 525 nm, with a red shift of 2–3 nm as compared to the starting Au15@citrate NPs (see Supporting Information (SI), Figure S1A), revealing a successful coating of each individual particle without aggregation, which was confirmed by the transmission electron microscopy (TEM) measurements (Figure S1B in SI). It is worth noting that the protein coated NPs were extremely stable in aqueous media, which highly facilitates the concentration of the dispersions to very high particle concentrations (50–100 mM Au^0) simply by centrifugation.

In the case of the 60 nm CTAB stabilized gold NPs[45] (Au60@CTAB), the procedure for the protein coating was slightly different. Here, the Au60@CTAB dispersion was rapidly mixed with a BSA/citrate solution, containing higher BSA concentration (0.1wt% citrate, $c(BSA)_{final}$ = 1 mg/mL) and immediately centrifuged at 3500 g until all the particles sedimented. The supernatant was replaced with a basic BSA solution (1 mg/mL BSA, 0.1wt% citrate, pH ≈ 9–10) and the mixture was shaken for 24h. The resulting particles were then purified and concentrated by centrifugation, similar to the Au15@BSA NPs. UV –vis-NIR spectroscopy (Figure S1C in SI) and TEM (Figure S1D in SI) revealed that also the Au60@CTAB NPs were successfully coated with the protein, without aggregation. The LSPR extinction maximum for the Au60@BSA NPs was found to be located at around 540 nm, similar to that of Au60@CTAB, revealing no significant refractive index changes in the vicinity of the Au NPs, before and after BSA coating (Figure S1C). For the citrate-coated NPs, we assume that the citrate is replaced almost completely by the protein, due to the weaker binding ability of citrate compared to a protein, which bears a large amount of strongly binding functional groups. Moreover, the displacement of citrate from the particle surface could also be favored by multiple washing steps at basic pH (see Experimental Section). However, for the CTAB-coated NPs, the protein might only partially replace the CTAB molecules, but could also adsorb on top of the positively charged CTAB bilayer via electrostatic interactions.

Proteins are typically very sensitive toward pH and exhibit U-shaped pH-solubility profiles with a minimum at the isoelectric point (pI).[25] The pI of BSA lies around pH 4.6-4.9.[33,48] Similar to pure BSA, both Au15@BSA and Au60@BSA were found to be highly pH-responsive and to exhibit U-shaped dispersibility as a function of solution pH, with a minimum around pH 4.5-5, which is consistent with the pI of BSA (**Figure 1**). At pH values below and above the pI(BSA), mainly in the range of 5.5 ≤ pH ≤ 3.5, the dispersions are red in color (Figure 1A) and perfectly stable, with an LSPR band maximum around 525 nm (Figure 1B, C), which means that the particles are well separated from each other. At pH = pI(BSA) the NPs were consistently found to aggregate as confirmed by the color of the dispersions,

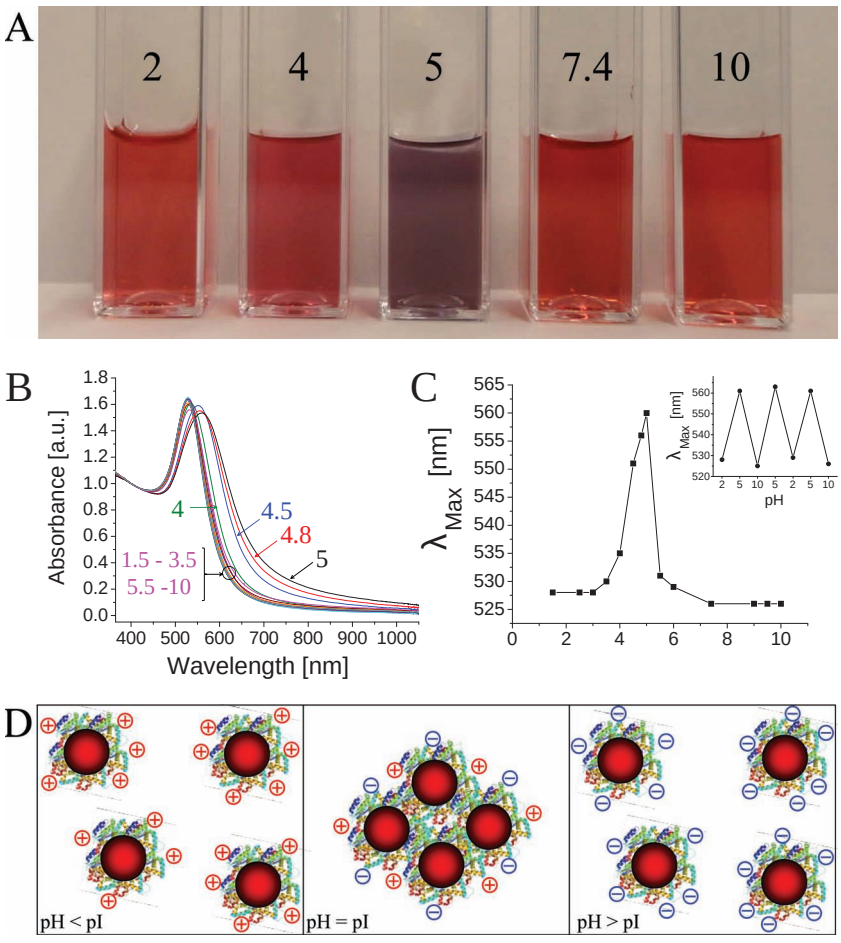

Figure 1. Reversible pH-responsive behavior of BSA coated NPs. A) Representative photograph of Au15@BSA NP-dispersions at different pH. The pH values are displayed on the vials. B) UV–vis–NIR spectra of Au15@BSA NPs at pH = 1.5, 2.5, 3, 3.5, 4, 4.5, 4.8, 5, 5.5, 6, 7.4, 9, 9.5 and 10. The NPs are colloidally stable at pH<pI>pH and aggregate at pH ~ pI, resulting in color change from deep red to purple (A) and a redshift of the LSPR band of around 30 nm (B and C). The pH-induced aggregation is completely reversible and can be repeated multiple times (C inset). D) Schematic illustration of the pH dependent charge inversion of the Au@BSA NPs from positive at pH<pI over neutral at pH = pI to negative at pH>pI. The pI of pure BSA is around 4.6-4.9.[33,48]

which changed from red (pH ≥ 7, Figure 1B) to violet/purple at pH ~5 (Figure 1B). The LSPR band of the NPs became broader and shifted to higher wavelengths with a total redshift of ~ 30 nm (Figure 1B, C). Upon increasing or decreasing the pH away from the pI, the particles disaggregated again and the color of the dispersions changed back to red (Figure 1A). Accordingly, the LSPR band regained its original shape and position with a maximum around 525 nm, indicating disaggregation of the NPs (Figure 1C, D). The pH-induced aggregation of the Au@BSA NPs is completely reversible and can be repeated multiple times, without having any effect on the colloidal stability of the NPs (Figure 1C inset).

At pH values close to the pI of a protein, the protein is usually less soluble in water. The solubility of proteins increases by decreasing or increasing the pH, due to the increased positive or negative net charge, respectively.[25] Therefore, at pH values below the pI_{BSA}, the Au@BSA NPs are expected to be positively charged and at pH values above the pI_{BSA}, the particles should be negatively charged, and hence, individually dispersed and perfectly stable as illustrated in Figure 1D and confirmed by ζ-potential measurements (**Figure 2**C, D). At pH values close to the pI, the particles do not bear a significant surface charge and the electrostatic repulsions between the NPs are thus not high enough to counteract the attractive forces, comprising van der Waals forces and the hydrophobic interactions between the non-polar side groups of the proteins, which ultimately results into aggregation and precipitation of the particles.[25] The point of zero charge of the Au@BSA NPs lies between pH 4 and 5, similar to the pI for pure BSA. Both UV–vis–NIR and ζ-potential data are consistent with this value (Figure 1B, C and Figure 2C, D).

As described above, upon decreasing the pH from 10 down to 2, the color of the Au@BSA NPs changes from red to purple/violet and then back to red. However, in the acidic pH range, i.e., pH ≤ 3.5, the LSPR band does not regain its shape completely and becomes slightly broader (Figure 1B) with the maximum around 528 nm (Figure 1C and 1C inset), indicating an incomplete disaggregation of the NPs to a minor degree. At high pH values, the surface charge of the Au@BSA NPs lies around -50 mV, implying high electrostatic repulsion between the NPs (Figure 2C, D). Moving toward low pH values, the surface charge of the NPs is inverted from negative to positive, with a ζ-potential around +20 mV at pH ~ 2 (Figure 2C, D). The relatively low surface charge at acidic pH could be the reason behind this incomplete disaggregation. Although a net charge of 30 mV is commonly accepted as the colloidal stability threshold for charged colloids,[49] the Au@BSA NPs still reveal a high colloidal stability under such acidic conditions, which is in contrast to our previously reported Au@insulin NPs.[11] Au@insulin NPs also revealed a pH-responsive behavior, however they did not show a U-shaped dispersibility profile, as in the case of Au@BSA NPs. Moving from pH 10 to pH 2, Au@insulin NPs consistently aggregated, changing their color from red (pH ≥ 7) to grey/blue at acidic pH and finally, precipitated. This variation in the pH-responsive behavior and stability under acidic conditions of the two protein-capped NPs (Au@BSA and Au@insulin) is likely related to the difference in molecular weights of the two proteins and therefore, to the additional steric stabilization stemming from the large BSA molecules,[33] as compared to the relatively very small insulin molecules.

Although proteins are highly sensitive to elevated temperatures and undergo denaturation and gelation,[27,35] Au@BSA NPs did not exhibit any of such behaviors. Denaturation is the process when proteins lose their 3-D tertiary structure due to the

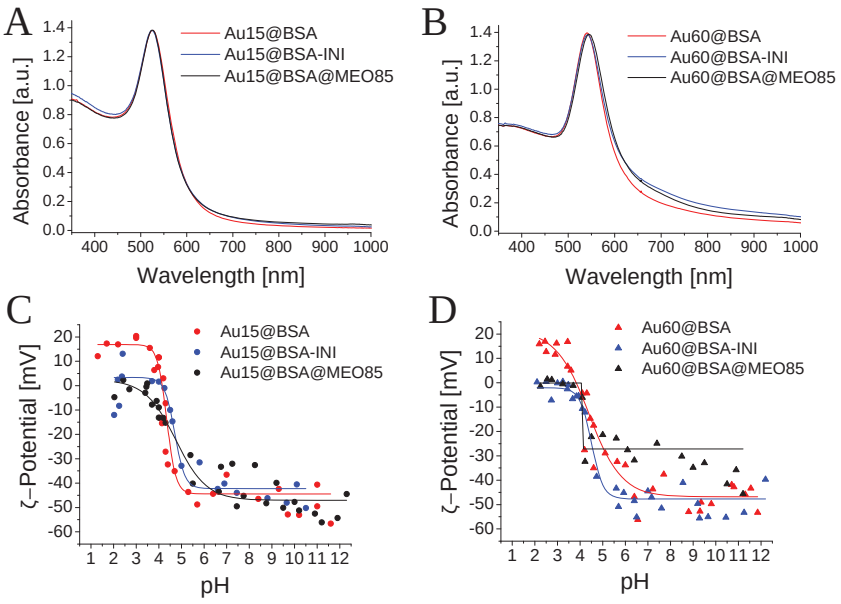

Figure 2. Characterization of 15 nm and 60 nm BSA-coated gold NPs grafted with the polymer brush of poly(MEO_2MA85-co-OEGMA15) after each reaction step according to Scheme 1. UV–vis-NIR spectra of Au15@BSA@MEO85 (A) and Au60@BSA@MEO85 (B) with their respective ζ-potential profiles (C and D). The solid lines in (C) and (D) are the sigmoidal fits (Boltzmann) of the respective ζ-potential profiles

conformational changes induced by extreme conditions such as high temperatures, whereas gelation is the process of protein coagulation/aggregation due to the increased inter-protein interactions under similar conditions. Proteins generally lose their tertiary structure when they adsorb on surfaces, and therefore BSA is already expected to be denaturated.[50] Furthermore, for gelation a certain protein concentration is required, usually c > 5% w/w,[27] which is not the case for protein-coated NPs. Therefore, both effects are supposed to play a negligible role for BSA-coated NPs and one should expect no temperature effect or at least to a minor degree. In fact, the Au@BSA NPs did not aggregate even when heated to 80 °C (see Figure S2 in SI). Therefore, in order to confer a switchable thermo-responsive behavior to the protein-coated NPs, a thermosensitive polymer brush was grafted on top of the protein layer. For this, first an ATRP-initiator (2-bromo-2-methyl iso-propylic acid bromide) was covalently attached on the BSA-coated NPs to the available amine groups of the protein, mainly the ε-amine groups of L-lysine, via an amide bond, as illustrated in Scheme 1. It is worth noting that the protein-coated NPs exhibit extremely high colloidal stability and further functionalization reactions, even under harsh conditions, do not affect the stability and the quality of the nanoparticles. The quality of the resulting Au@BSA-Ini NPs was monitored by UV –vis-NIR spectroscopy. No shift in the LSPR band of the Au@BSA-Ini NPs (both 15 and 60 nm NPs) was observed, as compared to Au@BSA, revealing that no aggregation occurred during the coupling reaction of the ATRP-initiator (Figure 2A and B). The pI (or the point of zero charge) of the Au@BSA-Ini NPs shifted slightly toward lower pH values and the ζ-potential of the NPs did not exceed +5 mV under acidic conditions, in contrast to the Au@BSA NPs, indicating the consumption of the amine groups of the protein, as a result of the initiator-coupling (Figure 2C and D).

In the final step, thermosensitive polymer brushes, consisting of random copolymers of MEO_2MA and OEGMA, (poly(MEO_2MAx-co-OEGMA100-x)), were "grafted from" the protein layer of the particles via SI-ATRP. These non-ionic polymers are biocompatible, as a result of the presence of ethylene glycol units on their side chains, but also thermosensitive, with an LCST that can be easily tuned by varying the molar ratio between the two monomers.[19,51] We grafted polymer brushes of MEO_2MA and OEGMA in a molar ratio of 85:15, (poly(MEO_2MA85-co-OEGMA15)), because this polymer exhibits an LCST of 42 °C in pure water at neutral pH, but of 37–38 °C, i.e. close to the body temperature, at physiological conditions (pH 7.4, ionic strength (I)= 0.15 mol/L). ATRP was conducted for 1-2 h in aqueous and in semi-aqueous mixtures (H_2O/DMF (1:1 v/v)) using Cu(I)Br/PMDETA as catalyst (see Experimental Section), in a high excess of the monomers. However, the semi-aqueous approach afforded higher reproducibility of the product, due to the better solubility of the monomers, higher stability of the catalyst in the H_2O/DMF mixture and more importantly, less coagulation of the NPs during the polymerization. The resulting NPs (Au15@BSA-MEOMA85 and Au60@BSA-MEOMA85) were characterized by UV-vis-NIR spectroscopy, ζ-potential measurements (Figure 2) and TEM (**Figure 3**). UV–vis-NIR spectroscopy revealed no significant shift in the LSPR band, again confirming that no particle aggregation occurred during the polymerization reaction (Figure 2A, B). TEM revealed individual particles with a dry organic layer of 3-4 nm in average, as shown in Figure 3A and B. The ζ-potential measurements revealed a similar pH profile to that of Au@BSA-Ini NPs, with ζ-potential values not

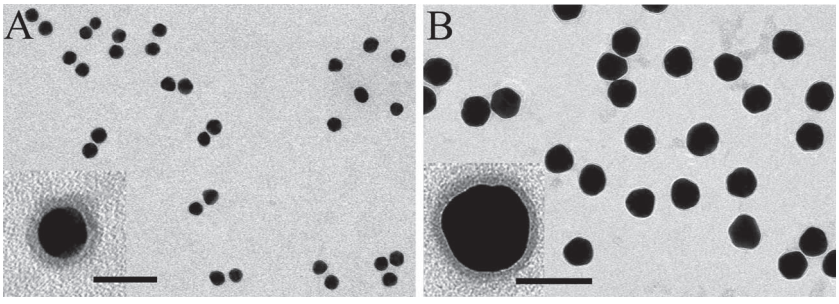

Figure 3. Transmission electron microscopy images of BSA-coated gold NPs grafted with the polymer brush of poly(MEO_2MA85-co-OEGMA15). A) Au15@BSA@MEO85 NPs. The scale bar represents 100 nm for the image and 20 nm for the inset. B) Au60@BSA@MEO85 NPs. The scale bar represents 200 nm for the image and 50 nm for the inset.

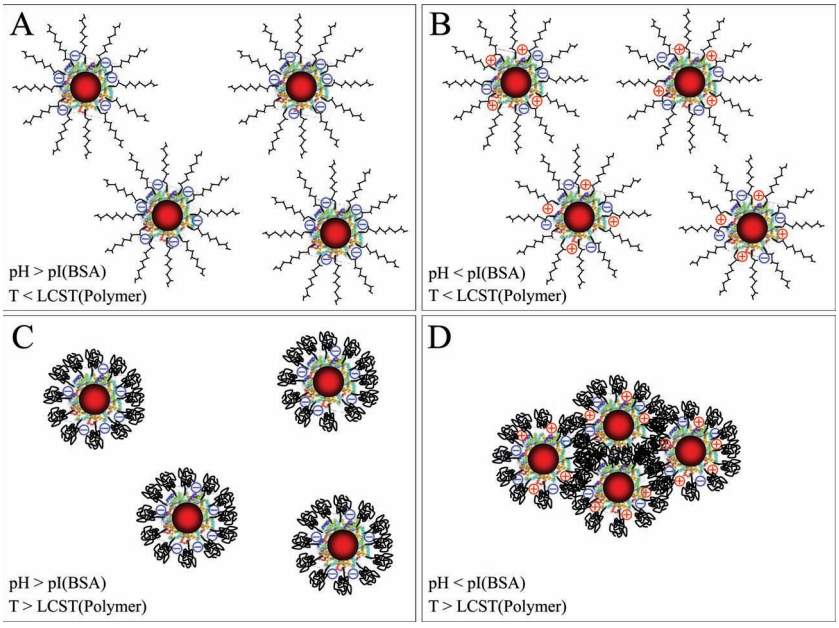

Scheme 2. pH-Dependent thermo-responsive behavior of BSA-coated gold NPs grafted with of poly(MEO_2MA85-co-OEGMA15) polymer brush. At pH > pI(BSA) the NPs are negatively charged (A and C) and at pH < pI(BSA) the NPs bear nearly no net charge (B and D). At T < LCST (A and B), the polymer brush is hydrophilic and stretched, conferring steric stability to the NPs. At T > LCST (C and D) the polymer brush is collapsed. At T > LCST and pH > pI (C), the NPs do not aggregate due to the electrostatic stabilization stemming from the protein layer, whereas at pH < pI (D) the NPs aggregate due to the lack of electrostatic repulsion and increased hydrophobic interactions.

exceeding 0 mV, again in contrast with the Au@BSA NPs (Figure 2C, D).

The Au@protein-*g*-polymer NPs of both sizes, Au15@BSA-MEOMA85 and Au60@BSA-MEOMA85 were expected to exhibit a pH-dependent thermosensitive behavior as illustrated in **Scheme 2**. Therefore, the effect of pH on the thermal response of both systems was examined by adjusting the pH of the dispersions to low (pH 2.5, no surface charge) and high (pH 10, high surface charge) values, followed by heating (above the LCST, 60 °C) and cooling (below the LCST, room temperature) cycles. At temperatures below the LCST (i.e. below 42 °C in H_2O or 37 °C in 0.15 M salt solution), the Au@BSA-MEOMA85 NPs are stable at all pH values. In particular, at pH values above the pI of the protein and temperatures below the LCST, where the protein layer is negatively charged, the particles experience both electrostatic repulsion from the protein layer and steric repulsion from the (swollen) polymer brush layer (Scheme 2A). The particle dispersions were indeed found to be red, with the LSPR band centered at 525 nm for the Au15@BSA-MEOMA85 NPs and at 540 nm for the Au60@BSA-MEOMA85 NPs, indicating the presence of well separated NPs (**Figure 4**A,C). At temperatures below the LCST and pH ≤ pI, where the protein layer bears a negligible net charge, the NPs are also stable, since the polymer brush layer prevents the NPs from aggregating (Scheme 2B). The particle dispersions still reveal red color with LSPR maxima of 525 nm or 540 nm respectively (Figure 4B,D). Above the LCST (60 °C), the polymer brush layer undergoes a hydrophilic/hydrophobic phase transition and collapses, as illustrated in Scheme 2C,D. However, at high pH values (pH 10), the NPs particles do not aggregate, which was confirmed by the red color and the LSPR wavelength of the dispersions (Figure 4A, C). In addition to this, dynamic light scattering (DLS) measurements (**Figure 5**) performed at different temperatures revealed that the average particle size even decreases slightly when increasing temperature, due to the collapse of the polymer brush layer (Figure 5, blue dots, see also the insets). Under these conditions, the stability arises from the protein layer, which is negatively charged, so that electrostatic repulsions still dominate (Scheme 2C). On the contrary, at low pH values (pH 2.5), where the protein layer bears no net charge (or low net charge, i.e. below +30 mV) and thus electrostatic repulsions are very weak, the particles do have the chance to come closer to each

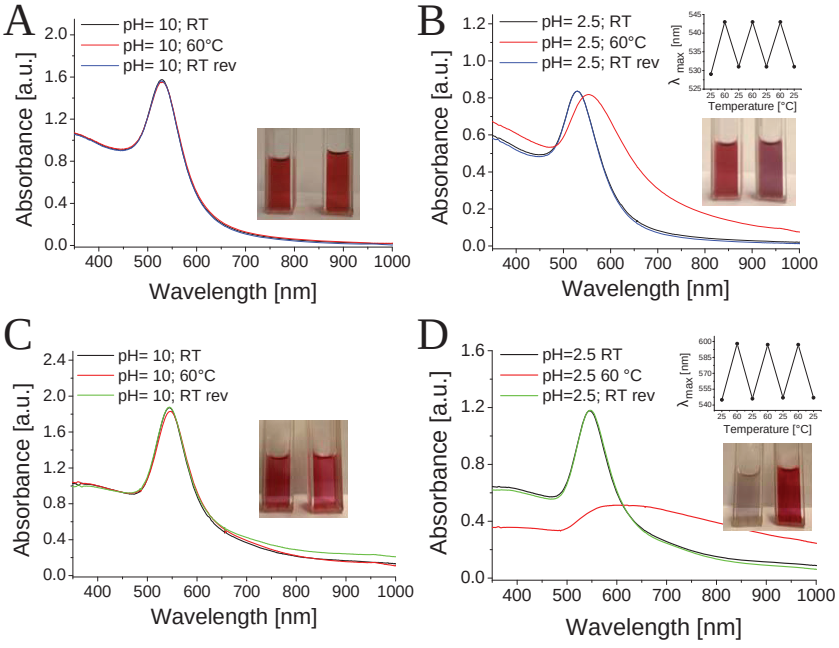

Figure 4. pH-dependent thermo-responsive behavior of 15 nm and 60 nm BSA-coated gold NPs grafted with poly(MEO_2MA85-co-OEGMA15) polymer brush. UV–vis–NIR spectra and photographs of Au15@BSA@MEO85 (A and B) and Au60@BSA@MEO85 (C and D) at T << LCST (RT) and T >> LCST (60 °C) at pH 10 (A and C) and 2.5 (B and D). At high pH the NPs are negatively charged and do not aggregate upon heating, whereas at low pH, the net surface charge is close to zero and reversible aggregation is observed at high temperature (above LCST). The process is completely reversible and can be repeated multiple times (graph insets in B and D).

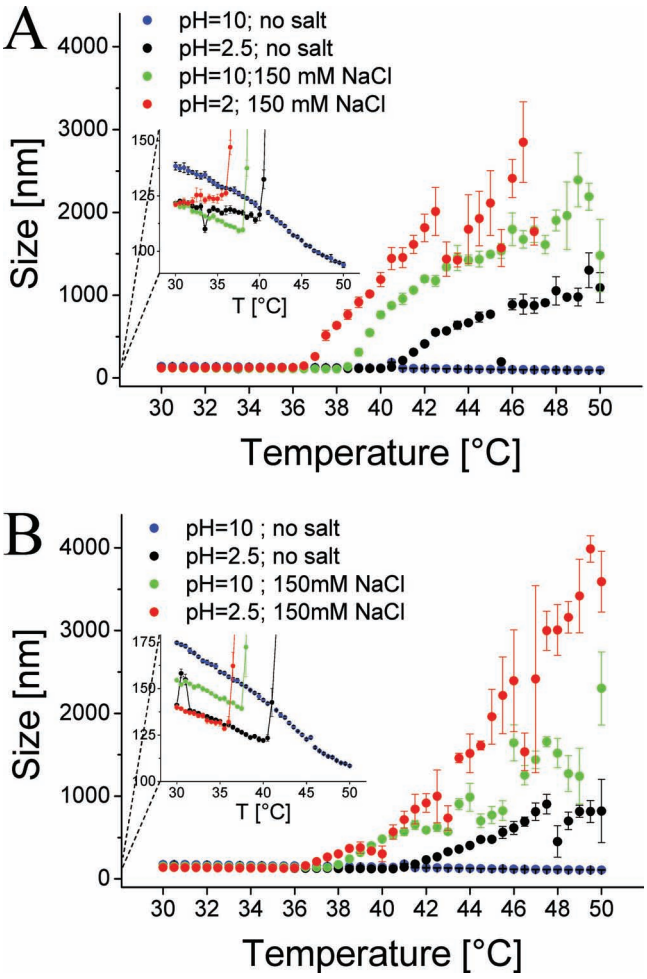

Figure 5. Average particle size (determined by DLS) of Au15@BSA@MEO85 (A) and Au60@BSA@MEO85 (B) as a function of temperature at pH below (pH 2.5) and above (pH 10) the pI of BSA, both in pure water and in 150 mM NaCl solution. The insets show a zoom for the range of small sizes.

other, which results into particle aggregation, due to the hydrophobic interactions between the polymer layers (Scheme 2D). Such aggregation can be visually observed through the color change due to LSPR coupling between NPs within the formed clusters (Figure 4B,D). As expected, the particles start aggregating at temperatures close to 42 °C in water, as confirmed by DLS (Figure 5, black dots). The dispersions become purple-blue in the case of 15 nm particles (Figure 4B image inset) and light grey in the case of 60 nm particles (Figure 4D image inset). The temperature-induced aggregation of the particles was completely reversible and could be repeated multiple times, without affecting the stability of the NPs (Figure 4B,D and the respective graph insets). However, at high ionic strength, both Au@15@BSA-MEOMA85 and Au60@BSA-MEOMA85 NPs aggregate when the temperature is increased, even at high pH values (Figure 5). Indeed, the electrolytes screen the electric double layer around the NPs, thus decreasing the electrostatic repulsions and facilitating particle aggregation. Additionally, the LCST of the polymers decreases in the presence of salt and therefore the NPs are found to aggregate at lower temperatures.[19] At pH 2.5, aggregation was observed around 40.5 °C in the absence of salt, but around 36.5 °C under physiological conditions (150 mM NaCl). At pH 10, the aggregation temperature was similarly around 37-38 °C, i.e. body temperature, at physiological salt concentration (Figure 5A, B).

3. Conclusions

In conclusion, we present a simple method for the synthesis of dual-responsive gold NPs, by grafting thermosensitive polymer brushes on protein-capped gold nanoparticles via SI-ATRP. The method can be used for spherical gold NPs of different size and surface chemistry (i.e., different stabilizing agents, namely citrate and CTAB) and thus we expect that it can be extended to other morphologies and compositions. In the examples shown here, the protein (BSA) imparted pH-sensitivity and extremely high colloidal stability to the NPs, but also a huge variety of chemical functionalities available for further modification of the particles, while the polymer brushes (poly(MEO_2MA85-OEGMA15)) provide thermal sensitivity, displaying an LCST of 42 °C in pure water and around 37 °C under physiological conditions. Thus, the protein-coated nanoparticles grafted with thermosensitive polymers exhibit an overall pH-dependent thermal sensitivity, with reversible aggregation (and optical changes) restricted to low pH values (below pI of the BSA), under salt-free conditions. Hence, Au@BSA-*g*-Poly(MEO_2MA-co-OEGMA) NPs represent a smart stimuli-responsive system, based on plasmonic particles coated with protein-polymer conjugates.

4. Experimental Section

Chemicals: Bovine serum albumin (BSA), poly(ethylene glycol) methylether methacrylate (OEGMA), 2-(2-methoxyethoxy)ethyl methacrylate (MEO_2MA), copper(I) bromide, 2-bromo-2-methyl isopropylic acid bromide (ATRP-Initiator), $HAuCl_4{\cdot}3H_2O$, trisodium citrate dihydrate and *N*,*N*,*N*′,*N*″,*N*″-Pentamethyldiethylenetriamine (PMDETA), N,N-dimethylformamide, methanol, glacial acetic acid, sodium carbonate and sodium hydroxide (pellets) were supplied by Sigma Aldrich. Hydrochloric acid (37%) and nitric acid (65%) were supplied by Panreac Life Sciences. Copper(I)bromide was washed multiple times with glacial acetic acid, followed by ethanol, and finally vacuum dried before use. All other reactants were used without further purification. All reaction vessels were washed with *aqua regia* before use.

Particle Synthesis: 15 nm citrate-capped gold NPs (Au15@citrate, 0.5 mM Au^0) were prepared by the citrate reduction method.[44] Briefly, 12 mL of a pre-warmed sodium citrate solution (1 wt%) was added to a boiling 238 mL $HAuCl_4$ solution ([$HAuCl_4$] = 0.525 mM) and boiled for about 10 minutes until the color changed to red. The particles with a diameter of 60 nm were synthesized through a seeded growth method, based on the reduction of $HAuCl_4$ with ascorbic acid in the presence of pre-synthesized Au15@citrate NPs in a 15 mM CTAB solution.[45] For this, first 1.16 mL of 15 nm NPs seed solution was mixed with the same volume of 30 mM CTAB solution. Then, to a mixture of 250 mL $HAuCl_4$/CTAB solution ([$HAuCl_4$] = 0.25 mM, [CTAB] = 15 mM), 250 µL of a 0.5 M ascorbic acid was added followed by the addition pre-prepared seed solution (final [Au^0] = 2.31 µM). The mixture was stirred at 35 °C for 24 hours. Prior to further usage, the spherical Au60@CTAB particles were separated from the non-spherical ones via CTAB assisted purification method.[45]

Synthesis of BSA-Coated Gold NPs: 15 nm BSA-coated gold NPs (Au15@BSA NPs) were synthesized by simply adding BSA/citrate solution (0.1%

citrate, pH ≈ 7) to the as-prepared Au15@citrate NP dispersions (0.5 mM Au^0) at room temperature, giving a final BSA concentration of 0.1 mg/mL. After a stirring time of 24 hours, the particles were purified and concentrated (5–10 mM Au^0) by several centrifugation/redispersion cycles (8500 g, 80 min) and stored at pH 8-9 at room temperature. It is worth noting that the Au15@BSA dispersions can also be concentrated to very high particle concentrations such as 50–100 mM Au^0, simply by centrifugation.

For the synthesis of Au60@BSA NPs, the NP concentration of Au60@CTAB was adjusted, having 0.5 mM Au and ~ 1mM CTAB. Then the particle dispersion was rapidly mixed with an equal volume of a BSA/citrate solution (0.1% citrate, pH ≈ 7) giving a final BSA concentration of 1 mg/mL and centrifuged immediately at 3500 g till all particles sedimented. The supernatant was replaced with a basic BSA/citrate solution (1 mg/mL BSA, 0.1% citrate, pH ≈ 9–10) and the mixture was shaken for 24 hours. The resulting particles were purified and concentrated (5–10 mM Au) by several centrifugation/redispersion cycles (3500 g, 30min) and stored at pH 8-9 at room temperature.

Synthesis of ATRP-Initiator-Functionalized Au@BSA NPs (Au15@BSA-Ini and Au60@BSA-Ini): The coupling reaction of the ATRP-Initiator, 2-bromo-2-methyl iso-propylic acid bromide, with the BSA-coated gold NPs was carried out in 0.15 M sodium carbonate buffered (~pH 9) aqueous dispersions of Au@BSA NPs. For this, 75 µL 2-bromoisobutyryl bromide was dissolved in 500 µL DMF and added dropwise to 15 mL Au@BSA dispersion ([Au15@BSA] = 8×10^{-4} M Au^0 that corresponds to ~ 6.9×10^{-10} M particles and [Au60@BSA] = 1.5×10^{-4} M Au^0 that corresponds to ~2.8×10^{-12} M particles). The solution was stirred at room temperature for 24 hours and washed 3 times by centrifugation (d = 15: 8500 g, 80 min; d = 60 nm: 3500 g, 30 min)

Grafting of poly(MEO_2MA85-co-OEGMA15) on Au@BSA-Ini NPs via SI-ATRP: For the polymerization, 10 mL particle solution ([Au15@BSA] = 4×10^{-4} M Au^0 that corresponds to ~ 3.4×10^{-10} M particles and [Au60@BSA] = 3×10^{-4} M Au^0 that corresponds to ~5.6×10^{-12} M particles) was diluted with 10 mL DMF. Then 3.4 mL MEO_2MA (3.4 mmol) and 1.4 mL OEGMA (0.6 mmol, ratio MEO_2MA/OEGMA 85/15) were added and the pH set to 9. Please note that the pH adjustment at this step is a very slow process. While adding base to the mixture, the pH increases rapidly and then decreases with time. Therefore, it is recommended to wait (at least 20 min) until the pH is constant, to avoid particle aggregation during the polymerization. The particle solution was then degassed under vacuum for 20 min before degassing for another 20 min under argon flow. In the meantime, 27 µL PMDETA was added to 1.5 mL of previously degassed methanol and again degassed under Argon for another 20 min. Then 3.1 mg CuBr was added and after the solution got slightly green to bluish, an amount of 0.6 mL was added to the particle solution. The polymerization was carried out for 1 h (2 hours for the 60 nm Au NPs), and aborted by exposing the mixture to air. The particles were purified by 4-fold centrifugation (for d = 15 nm: 8500 g, t = 80 min; for d = 60 nm: 3500 g, t = 30 min).

Characterization: Transmission electron microscopy (TEM) was carried out with a JEOL JEM 1010 transmission electron microscope operating at an acceleration voltage of 100 kV. UV–vis-NIR spectra were measured with a Cary 5000 UV–vis-NIR spectrophotometer. ζ-potential values were determined through electrophoretic mobility measurements using a Malvern Zetasizer Nano ZS Zen3600 by taking the average of five measurements, each consisting of at least 50 runs. Temperature dependent dynamic light scattering (DLS) measurements were also peformed on a Malvern Zetasizer Nano ZS, by taking the average of 5 measurements of 15 runs each for each temperature. The temperature intervals were of 0.5 °C and temperature equilibration time of 10 minutes. pH measurements were performed with Crison Micro pH-2000 pH-meter. Photographs were recorded with a Sony DSC-W350 digital camera.

Supporting Information

Supporting Information is available from the Wiley Online Library or from the author.

Acknowledgements

The authors acknowledge the EU (METACHEM, grant number CP-FP 228762-2), Spanish Ministerio de Ciencia e Innovación/FEDER (CTQ2010-18576 and MAT2010-15374), Xunta de Galicia/FEDER (10PXIB314218PR and 09TMT011314PR) and the Graduate School of Excellence "Material Science in Mainz" for financial support.
This article was amended on April 10, 2012 to correct typographical errors in Scheme 1 and Figure 5 that were present in the version originally published online.

Received: October 13, 2011
Revised: December 5, 2011
Published online: January 30, 2012

[1] M. A. C. Stuart, W. T. S. Huck, J. Genzer, M. Muller, C. Ober, M. Stamm, G. B. Sukhorukov, I. Szleifer, V. V. Tsukruk, M. Urban, F. Winnik, S. Zauscher, I. Luzinov, S. Minko, *Nat. Mater.* **2010**, *9*, 101.
[2] Y. Shen, M. Kuang, Z. Shen, J. Nieberle, H. W. Duan, H. Frey, *Angew. Chem. Int. Ed.* **2008**, *47*, 2227.
[3] I. Tokarev, S. Minko, *Adv. Mater.* **2009**, *21*, 241.
[4] S. T. Selvan, T. T. Y. Tan, D. K. Yi, N. R. Jana, *Langmuir* **2010**, *26*, 11631.
[5] a) C. D. H. Alarcon, S. Pennadam, C. Alexander, *Chem. Soc. Rev.* **2005**, *34*, 276; b) D. Schmaljohann, *Adv. Drug Delivery Rev.* **2006**, *58*, 1655; c) S. F. Medeiros, A. M. Santos, H. Fessi, A. Elaissari, *Int. J. Pharm.* **2011**, *403*, 139.
[6] M. Motornov, R. Sheparovych, R. Lupitskyy, E. MacWilliams, S. Minko, *Advanced Materials* **2008**, *20*, 200.
[7] a) M. Motornov, S. Minko, K. J. Eichhorn, M. Nitschke, F. Simon, M. Stamm, *Langmuir* **2003**, *19*, 8077; b) S. Minko, *Polym. Rev. (Philadelphia, PA, U. S.)* **2006**, *46*, 397.
[8] M. Motornov, Y. Roiter, I. Tokarev, S. Minko, *Prog. Polym. Sci.* **2010**, *35*, 174.
[9] a) A. Kaiser, T. Gelbrich, A. M. Schmidt, *J. Phys.: Condens. Matter* **2006**, *18*, S2563; b) M. Q. Zhu, L. Q. Wang, G. J. Exarhos, A. D. Q. Li, *J. Am. Chem. Soc.* **2004**, *126*, 2656; c) D. J. Li, X. Sheng, B. Zhao, *J. Am. Chem. Soc.* **2005**, *127*, 6248.
[10] a) J. Ruhe, M. Ballauff, M. Biesalski, P. Dziezok, F. Grohn, D. Johannsmann, N. Houbenov, N. Hugenberg, R. Konradi, S. Minko, M. Motornov, R. R. Netz, M. Schmidt, C. Seidel, M. Stamm, T. Stephan, D. Usov, H. N. Zhang, in *Polyelectrolytes with Defined Molecular Architecture I*, Vol. *165* (Ed: M. Schmidt), **2004**, *79*; b) M. Tomasulo, I. Yildiz, F. M. Raymo, *J. Phys. Chem. B* **2006**, *110*, 3853.
[11] M. Chanana, M. A. Correa-Duarte, L. M. Liz-Marzán, *Small* **2011**, *7*, 2650.
[12] Y. J. Kim, R. C. Johnson, J. T. Hupp, *Nano Lett.* **2001**, *1*, 165.
[13] C. H. Luo, F. Zuo, Z. H. Zheng, X. Cheng, X. B. Ding, Y. X. Peng, *Macromol. Rapid Commun.* **2008**, *29*, 149.
[14] D. Diaz Diaz, D. Kuhbeck, R. J. Koopmans, *Chem. Soc. Rev.* **2011**.
[15] Y. C. Gan, J. F. Yuan, X. J. Liu, P. Wang, Q. Y. Gao, *J. Bioact. Compat. Polym.* **2011**, *26*, 173.
[16] M. Motornov, R. Sheparovych, R. Lupitskyy, E. MacWilliams, O. Hoy, I. Luzinov, S. Minko, *Adv. Funct. Mater.* **2007**, *17*, 2307.
[17] W. P. Lv, S. Q. Liu, X. B. Fan, S. L. Wang, G. L. Zhang, F. B. Zhang, *Macromol. Rapid Commun.* **2010**, *31*, 454.
[18] W. Z. Yuan, Z. D. Zhao, J. Y. Yuan, S. Y. Gu, F. B. Zhang, X. M. Xie, J. Ren, *Polym. Int.* **2011**, *60*, 194.
[19] M. Chanana, S. Jahn, R. Georgieva, J. F. Lutz, H. Baumler, D. Y. Wang, *Chem. Mater.* **2009**, *21*, 1906.
[20] E. W. Edwards, M. Chanana, D. Wang, H. Mohwald, *Angew. Chem. Int. Ed.* **2008**, *47*, 320.
[21] R. Contreras-Cáceres, J. Pacifico, I. Pastoriza-Santos, J. Pérez-Juste, A. Fernández-Barbero, L. M. Liz-Marzán, *Adv. Funct. Mater.* **2009**, *19*, 3070.

[22] Y. X. Liu, W. X. Tu, D. P. Cao, *Ind. Eng. Chem. Res.* **2010**, *49*, 2707; D. X. Li, Y. Cui, K. W. Wang, Q. He, X. H. Yan, J. B. Li, *Adv. Funct. Mater.* **2007**, *17*, 3134.
[23] G. Caetano-Anolles, M. W. Wang, D. Caetano-Anolles, J. E. Mittenthal, *Biochem. J.* **2009**, *417*, 621.
[24] E. M. P. Widmark, *Biochem. J.* **1923**, *17*, 668.
[25] D. H. G. Pelegrine, C. A. Gasparetto, *Lebensm.-Wiss. Technol.* **2005**, *38*, 77.
[26] N. Matsudomi, D. Rector, J. E. Kinsella, *Food Chem.* **1991**, *40*, 55.
[27] A. Tobitani, S. B. Ross Murphy, *Macromolecules* **1997**, *30*, 4845.
[28] J. Porath, J. Carlsson, I. Olsson, G. Belfrage, *Nature* **1975**, *258*, 598.
[29] F. Chai, C. Wang, T. Wang, Z. Ma, Z. Su, *Nanotechnology* **2010**, *21*, 025501.
[30] D. Aili, R. Selegard, L. Baltzer, K. Enander, B. Liedberg, *Small* **2009**, *5*, 2445.
[31] T. Yang, Z. Li, L. Wang, C. L. Guo, Y. J. Sun, *Langmuir* **2007**, *23*, 10533.
[32] a) D. H. Hu, Z. H. Sheng, P. Gong, P. F. Zhang, L. T. Cai, *Analyst* **2010**, *135*, 1411; b) A. Housni, M. Ahmed, S. Y. Liu, R. Narain, *J. Phys. Chem. C* **2008**, *112*, 12282.
[33] S. H. Brewer, W. R. Glomm, M. C. Johnson, M. K. Knag, S. Franzen, *Langmuir* **2005**, *21*, 9303.
[34] T. H. L. Nghiem, T. H. La, X. H. Vu, V. H. Chu, T. H. Nguyen, Q. H. Le, E. Fort, Q. H. Do, H. N. Tran, *Adv. Nat. Sci: Nanosci. Nanotechnol.* **2010**, *1*, 025009.
[35] R. Wetzel, M. Becker, J. Behlke, H. Billwitz, S. Bohm, B. Ebert, H. Hamann, J. Krumbiegel, G. Lassmann, *Eur. J. Biochem.* **1980**, *104*, 469.
[36] a) D. Popescu, H. Keul, M. Moller, *React. Funct. Polym.* **2010**, *70*, 767; b) C. Wang, R. J. Stewart, J. Kopecek, *Nature* **1999**, *397*, 417; c) H. D. Maynard, K. L. Heredia, R. C. Li, D. P. Parra, V. Vazquez-Dorbatt, *J. Mater. Chem.* **2007**, *17*, 4015.
[37] K. Matyjaszewski, J. H. Xia, *Chem. Rev. (Washington, DC, U. S.)* **2001**, *101*, 2921.
[38] S. Edmondson, V. L. Osborne, W. T. S. Huck, *Chem. Soc. Rev.* **2004**, *33*, 14.
[39] J. Pyun, S. J. Jia, T. Kowalewski, G. D. Patterson, K. Matyjaszewski, *Macromolecules* **2003**, *36*, 5094.
[40] C. Perruchot, M. A. Khan, A. Kamitsi, S. P. Armes, T. von Werne, T. E. Patten, *Langmuir* **2001**, *17*, 4479.
[41] E. Marutani, S. Yamamoto, T. Ninjbadgar, Y. Tsujii, T. Fukuda, M. Takano, *Polymer* **2004**, *45*, 2231.
[42] J. B. Kim, M. L. Bruening, G. L. Baker, *J. Am. Chem. Soc.* **2000**, *122*, 7616.
[43] M. Grzelczak, J. Pérez-Juste, P. Mulvaney, L. M. Liz-Marzán, *Chem. Soc. Rev.* **2008**, *37*, 1783.
[44] J. Turkevich, P. C. Stevenson, J. Hillier, *Discuss. Faraday Soc.* **1951**, 55.
[45] J. Rodriguez-Fernández, J. Pérez-Juste, F. J. G. de Abajo, L. M. Liz-Marzán, *Langmuir* **2006**, *22*, 7007.
[46] a) T. Peters, *Adv. Protein Chem.* **1985**, *37*, 161; b) K. Hirayama, S. Akashi, M. Furuya, K. Fukuhara, *Biochem. Biophys. Res. Commun.* **1990**, *173*, 639.
[47] D. Astruc, F. Lu, J. R. Aranzaes, *Angew. Chem. Int. Ed.* **2005**, *44*, 7852.
[48] J. M. Park, B. B. Muhoberac, P. L. Dubin, J. L. Xia, *Macromolecules* **1992**, *25*, 290.
[49] R. Xu, Ed. *Particle Characterization: Light Scattering Methods*, Kluwer Academic Publishers, Dordrecht, Netherlands **2000**.
[50] J. H. Teichroeb, J. A. Forrest, L. W. Jones, *Eur. Phys. J. E* **2008**, *26*, 411.
[51] J. F. Lutz, *J. Polym. Sci., Part A: Polym. Chem.* **2008**, *46*, 3459.